Natural Hazards (2021) 105:2777–2797
https://doi.org/10.1007/s11069-020-04423-9

ORIGINAL PAPER

Spatial and temporal variation of rainfall extremes for the North Anhui Province Plain of China over 1976–2018

Mingcheng Du[1,2] · Jianyun Zhang[1,2,3,4] · Qinli Yang[5] · Zhenlong Wang[6,7] · Zhenxin Bao[2,3,4] · Yanli Liu[2,3,4] · Junliang Jin[2,3,4] · Cuishan Liu[2,3,4] · Guoqing Wang[2,3,4]

Received: 14 August 2020 / Accepted: 6 November 2020 / Published online: 24 November 2020

Abstract
The North Anhui Province Plain (NAHPP), an important food production plain in China, is prone to frequent droughts and floods. To better understand the extreme events and mitigate their effects, this paper explores the spatiotemporal variation of precipitation extremes in the NAHPP during 1976 and 2018. Variation trends and spatial distributions of the annual maximum 1-day, 3-day, 7-day, and 15-day-rainfall were analyzed, and the probability distribution of rainfall extremes in the NAHPP was calculated by three distribution functions (Gumbel, P-III, and generalized extreme value). The optimal fitting function was selected based on the Kolmogorov–Smirnov test, and the rainfall in different return periods was calculated according to the optimal fitting function. The results indicate that rainfall extreme showed a 2- to 3-year periodicity on the interannual scale and 21-year periodicity on the chronological scale in the NAHPP. The rainfall extremes showed nonsignificant increase trend over the NAHPP, and some stations showed no significant decrease trend. The P-III distribution function best fit to the rainfall extremes (the maximum 1-day rainfall: 59%). The spatial distributions of rainfall extremes were similar in different return periods. As the return period increased, the estimated rainfall by the three distribution functions were slightly larger than that in the empirical return period. The findings will benefit regional water resources management and water-related risk control.

Keywords Rainfall extremes · Probability distribution · Return period · The North Anhui Province Plain · China

1 Introduction

With the development of global socioeconomy over the past decades, human-induced greenhouse gas emissions has changed the composition of the atmosphere and caused global warming, which has greatly affected the extreme precipitation and temperature events, especially for floods and droughts (Sarhadi and Soulis 2017; Diffenbaugh et al. 2017; Boukhelifa et al. 2018; Tong et al. 2020). According to the IPCC fifth assessment

✉ Guoqing Wang
gqwang@nhri.cn

Extended author information available on the last page of the article

report, the frequency of heavy precipitation events has increased in most land areas (IPCC 2013; Wang and Tian 2010). The increasing frequency of extreme events brings severe challenges to regional flood control safety and engineering design (Song et al. 2018). Simultaneously, the occurrence of extreme rainfall events has caused considerable damage to human life and property, the most serious of which is urban waterlogging (Duan et al. 2014). However, these extreme events show high spatiotemporal heterogeneity (Du et al. 2014; Soltani et al. 2016; Ntegeka and Willems 2008; McAfee et al. 2013; Panthou et al. 2014). For instance, a significant increase of the annual maximum 1-day rainfall is found in the global scope (Min et al. 2011; Westra et al. 2013). Extreme precipitation and the average intensity of extreme precipitation are increasing in China (Wang and Tian 2010; Wu et al. 2018; Ge et al. 2019). Jung et al. (2011) studied the rainfall data from 183 meteorological stations in South Korea and found that the annual precipitation data showed a significant increasing trend and the extreme rainfall series had strong spatial variability. Investigating extreme events in India, Guhathakurta et al. (2011) noted that heavy rainfall occurred less frequently in most parts of central and northern India while more frequently in eastern and northeastern India, with extreme precipitation and flood risks in the country increasing dramatically. Understanding the temporal and spatial variation of extreme rainfall plays a vital role in formulating effective and appropriate water resources management policies, especially in mitigating and preventing flood disasters (Jung et al. 2017; Fan et al. 2018; Wu et al. 2020).

How to represent the extreme rainfall events has attracted much attention. Most previous studies take the annual maximum daily rainfall or the maximum threshold method (Peak-Over-Threshold (POT)) to study extreme rainfall (Ntegeka and Willems 2008; Song et al. 2018). Some scholars argued that the variety of sub-daily extreme precipitation may be greater than that of the daily extreme under anthropogenic forcing (Olsson et al. 2015; Hosseinzadehtalaei et al. 2019). However, due to data limitation, it is difficult to quantify the change of extreme precipitation in sub-daily precipitation, especially on a large-scale basin (Hosseinzadehtalaei et al. 2020). In this study, the annual maximum 1-day, 3-day, 7-day, and 15-day rainfall are selected as evaluation indicators to analyze the changes in extreme events. Since these indicators reflect the frequent impact of extreme events on society, which in turn are used to predict rainfall in different return periods (Min et al. 2011).

Statistical methods can be used to predict the rainfall in different return periods so as to provide a reference for flood prevention in the future. The most commonly used probability distribution models are Gumbel, P-III, generalized extreme value (GEV), and generalized Pareto (GP) (Fischer et al. 2012; Xia et al. 2012; Coronado-Hern A Ndez et al. 2020; Samuel et al. 2020). For instance, Samuel et al. (2020) reported that Kaduna's monthly rainfall data are fitted to a generalized extreme value distribution. Mo et al. (2019) believed that the parameters of the GP and GEV models are variable in a climate change environment, and the fitting results of the GP model are better than the GEV model. Park et al. (2011) used Gumbel distribution and GEV distribution to study the variation of rainfall extreme values in South Korea. Chaudhuri and Sharma (2020) indicated that compared with Gumbel, GEV predicts the higher intensity of extreme rainfall with different return periods and duration in Delhi, India. The extreme rainfall distribution functions widely used in China in recent decades were Gamma and P-III type distribution functions (Hanson and Vogel 2008; Fischer et al. 2012; Xia et al. 2012). Wang et al. (2008) used Gamma distribution and K-S test to detect the variation of extreme precipitation in southern China. Xia et al. (2012) used GEV, Gamma, and GP models to analyze the extreme precipitation in the HRB and found that the annual maximum series can be better applied to GEV model, and the POT series can be better applied to GP model.

The North Anhui Province Plain (NAHPP) is located in middle reaches of the Huaihe River Basin (HRB), belonging to the north–south transitional zone in China. The HRB is a sensitive area to climate change (Ye and Li 2017) and a prone area to floods. In the twentieth century, the probability of flood in the HRB ranked the second in China (Duan et al. 2014). Its unique geographical location and frequent floods exert negative effects on crop growth in Anhui, which is a major agricultural province in China (Wei and Zhang 2010). Yang et al. (2016) and Ye and Li (2017) reported that the leading cause of the frequent floods in the HRB is the increase of extreme rainfall events or continuous heavy rainfall events. However, research on extreme rainfall in the HRB remains limited, and few scholars considered the variation and a probability distribution of extreme precipitation in the NAHPP (Xia et al. 2012; Yin et al. 2016; Ye and Li 2017). Located in the middle of the HRB, the NAHPP is the most vulnerable area being frequently hit by flood disasters induced by extreme rainfall. Taking the serious flood event in 2020 as an example, flood in the Huaihe River needs to be released to the NAHPP to alleviate the flood control pressure. As a result, flood in the NAHPP caused numerous economic losses, a large number of fields submerged and agricultural production reduced.

This paper aims to analyze the spatial and temporal variation of extreme precipitation in the NAHPP and study the statistical characteristics of extreme precipitation. The main objectives of this study are as follows: (1) to identify the oscillation period of rainfall at different time scales for the study area; (2) to investigate the spatial distribution and variation trend of different rainfall extremes over the study area; and (3) to estimate the return period of the rainfall extremes by using the optimal fitting distribution function. The findings would provide scientific support for flood control and disaster mitigation for the NAHPP.

2 Materials and methods

2.1 Study area and data sources

The NAHPP (Fig. 1) lies in the north of Anhui Province (114°55′ ~ 118°10′ E, 32°25′ ~ 34°35′ N), located in the middle reach of the HRB. It encompasses 6 cities and 27 counties (districts) of Bengbu, Huainan, Fuyang, Bozhou, Huaibei, and Suzhou. It covers about 3.9×10^4 km^2, accounting for about 30% of the total area of Anhui Province. The terrain is flat, except for a few hills in the north. The altitude ranges from 20 to 40 m, and the natural gradient is 1/7500 ~ 1/10,000. The region belongs to the warm temperate zone and the semi-humid monsoon zone, with dry winters and dry springs, and the same period of rain and heat. It has the transitional nature of the temperate and subtropical climate, with frequent meteorological disasters. Rainfall in the flood season (June to September), mostly in the form of heavy rain, accounts for 60–70% of the annual rainfall (Chen et al. 2018).

Rainfall data at 61 rainfall stations from 1976 to 2018 in the NAHPP were collected from the local water conservancy bureaus. As shown in Fig. 1, the rainfall station distribution in the NAHPP is relatively uniform. To analyze the spatial heterogeneity of rainfall distribution in the region, the study area was divided into three regions by using the K-means cluster analysis (KCA) method (Amiri and Mesgari 2016). Region I covers 17 rainfall stations with the least rainfall, Region II includes 26 stations, and Region III contains 18 stations with the heaviest rainfall (Fig. 1).

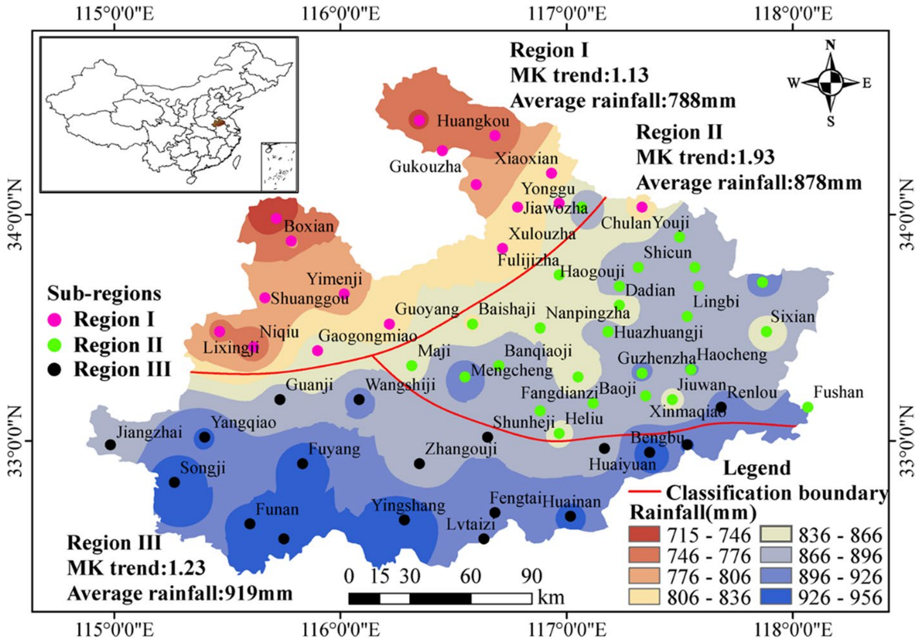

Fig. 1 Location of rainfall gauges and segment of the study area

2.2 Time series analysis

In this study, the ensemble empirical mode decomposition (EEMD) method was used to analyze the multi-scale rainfall so as to determine the oscillation mode structure characteristics of rainfall at different time scales. The EEMD is one of the methods to extract signals of changing trends and can assess the complex change of non-stationary signals (Wu and Huang 2009). It is an improvement in the empirical mode decomposition (EMD) method by adding an appropriate white noise to the original data and calculating the average of the set after many times (Huang et al. 2009). In this paper, the EEMD calculation process involved 1000 sets of samples, and the added amplitude of white noise was 20% of standard deviation for the synthetic sequence.

The Mann–Kendall (MK) trend test is a nonparametric test method that has been widely used in the trend test of hydrological and meteorological data series (Wang et al. 2017; Merabti et al. 2018; Dinpashoh et al. 2019). In this paper, it was used to analyze the variation trend of rainfall extreme values at various rainfall stations in the NAHPP. For a given time series $\{x_i\}$, where $i=1, 2,\ldots, n$, the calculation is as follows:

$$S = \sum_{k=1}^{n-1} \sum_{i=k+1}^{n} \operatorname{sign}(x_i - x_k) \tag{1}$$

$$\operatorname{sign}(x_i - x_k) = \begin{cases} +1 & \text{if } (x_i - x_k) > 0 \\ 0 & \text{if } (x_i - x_k) = 0 \\ -1 & \text{if } (x_i - x_k) < 0 \end{cases} \tag{2}$$

S statistics variance calculation method:

$$\operatorname{Var}(S) = \frac{n(n-1)(2n+5)}{18} \tag{3}$$

The standard normal statistical variable Z is:

$$Z = \frac{S - \operatorname{sign}(S)}{\sqrt{\operatorname{Var}(S)}} \tag{4}$$

The trend is statistically significant at $\alpha = 0.05$ significance level when $|Z| > 1.96$. When $Z > 1.96$, the sequence showed a significant increase, and when $Z < -1.96$, the sequence showed a significant decrease.

2.3 Distribution function

In this paper, three distribution functions (Gumbel, P-III, and GEV distribution) were used to simulate and fit the rainfall extreme value series. The applicability of the three distribution functions to different extreme precipitation in the NAHPP was studied, and the optimal fitting function used to calculate the rainfall extremes distribution in different return periods.

2.3.1 Gumbel

The Gumbel distribution function is:

$$F(x) = P(X < x) = \exp\left\{-\left[\exp\left(-\frac{x-\beta}{\alpha}\right)\right]\right\} \tag{5}$$

The parameters are estimated by the classical moment method, and the results are as follows: (Rahman et al. 2013; Qian et al. 2018):

$$\alpha = \frac{\mu_x}{\mu_y} = \frac{\sqrt{6}}{\pi}\sigma_x \tag{6}$$

$$\beta = E(x) - \alpha E(y) = E(x) - c * \frac{\pi}{\sqrt{6}}\sigma_x \tag{7}$$

α(scale parameter) and β(position parameter) are unknown parameters, determined according to the measured data; c is the Euler constant, with a value of 0.5772;σ_x is the standard deviation of sequence x; $E(x)$ is the mean value of sequence x.

2.3.2 P-III

The P-III curve is an unsymmetrical unimodal, positive deflection curve, and its distribution function is:

$$F(x) = \frac{1}{\alpha\Gamma(\gamma)} \int_{0}^{+\infty} \left(\frac{x-\beta}{\alpha}\right)^{\gamma-1} \exp\left(-\left(\frac{x-\beta}{\alpha}\right)\right) \mathrm{d}x \tag{8}$$

The lower formula can be obtained by the standardized transformation of the upper formula, and then, the rainfall can be calculated according to the design frequency (Jin et al. 2019):

$$x_p = \overline{x}(1 + C_v^2 \times C_s/C_v \times \text{Gammainv}\ (1-p,\ \alpha,\ \beta)/2 - 2C_v/C_s) \tag{9}$$

where γ(shape parameter) is an unknown parameter; $\Gamma(\gamma)$ is a Gamma function.

2.3.3 GEV

The GEV distribution function is:

$$F(x) = \exp\left\{-\left[1-\gamma\left(\frac{x-\beta}{\alpha}\right)\right]^{\frac{1}{\gamma}}\right\} \tag{10}$$

According to the above calculation, the rainfall in different return periods can be compared with the results of the empirical return period. For the calculation of the empirical return period, please refer to the Cunnane formula (Cunnane 1978; Song et al. 2018):

$$T = \frac{1}{\frac{n}{N}\left(1 - \frac{i-0.4}{n+0.2}\right)} \tag{11}$$

where n is the sample number of extreme sequences and N is the total number of years of extreme sequence, $i = 1, 2 \ldots n$.

2.4 Goodness-of-fit tests

The Kolmogorov–Smirnov (K-S) test was used to test the goodness of fit of the distribution function, which reflects the nonparametric test method of the degree of deviation between the hypothesis and the real population distribution (Shu et al. 2017). It is mainly to compare the theoretical distribution and empirical distribution to determine the maximum difference value D between them. The smaller D value means the better the fitting result. The trend is statistically significant at $\alpha = 0.05$ significance level when $D < D_\alpha = 0.208$. If more than one distribution function satisfies this condition, the distribution with the smallest D value will be taken as the optimal fitting distribution. Some researchers use root mean square error (RMSE) to judge the goodness of fit (Qian et al. 2018), but the principle is basically the same.

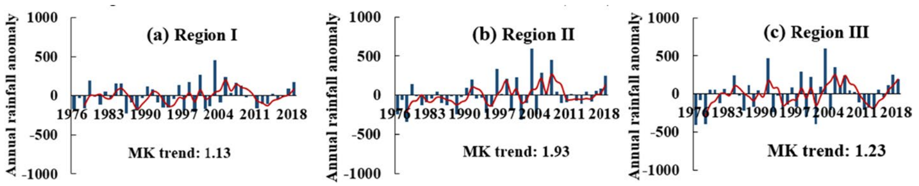

Fig. 2 Temporal evolution of annual rainfall anomaly in region I (**a**), region II (**b**) and region III (**c**). The red lines are the 3-year moving average curve, and the blue bars are the annual rainfall anomaly

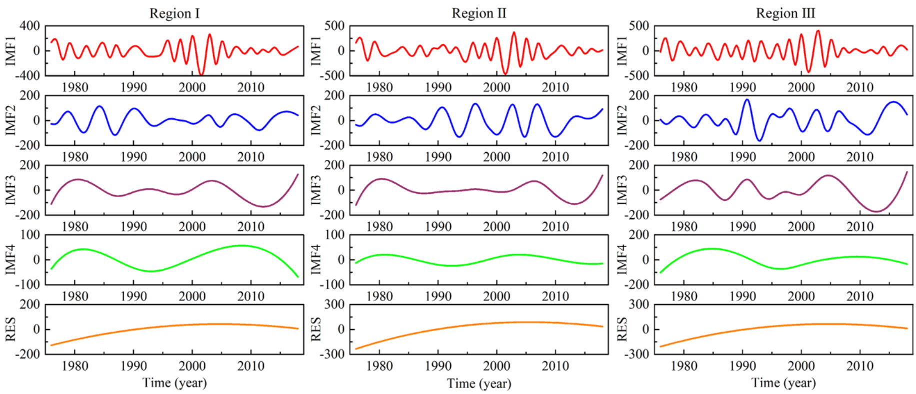

Fig. 3 Decomposition of annual rainfall anomaly time series in three subregions using EEMD

3 Results and discussions

3.1 Temporal and spatial variation of annual rainfall

The annual rainfall in the NAHPP is unevenly distributed and gradually decreases from south to north. Based on the MK test, the annual rainfall variation of each subregion was calculated and illustrated in Fig. 2. It indicates that the annual rainfall of the three subregions has no significant increasing trend, which is consistent with the results of Jin et al. (2014).

To obtain the characteristics of the annual rainfall variations on different time scales, the EEMD was applied to the annual rainfall anomaly of each subregion. The three original precipitation anomaly series are broken down into four IMF components and a trend term RES (Fig. 3). Each IMF component reflects the fluctuation characteristics at different time scales from high to low frequency, and the trend term shows the trend of the original data over time. The four IMF components in Fig. 3 were analyzed to obtain the oscillation period and the variance contribution rate (Table 1). The contribution of the oscillation period of 2.2–2.3 years to the rainfall anomaly was the largest (more than 58%). On the interannual scale, precipitation in Regions I and II showed 3-year (IMF1) and 6-year (IMF2) climate variability, and precipitation in Region III showed 3-year (IMF1) and 4-year (IMF2) climate variability. On a chronological scale, the three subregions had climate variability of 21 years (IMF3 and IMF4). The results are consistent with the Morlet wavelet analysis of Wei et al. (2010). The interdecadal oscillation of summer precipitation

Table 1 Major cycles and variance contribution rates of each component of annual rainfall anomaly series in the NAHPP from 1978 to 2018

IMF component of precipitation series	IMF1	IMF2	IMF3	IMF4	RES
Region I					
Major cycles (a)	2.33	6	21	21	
Variance contribution rates (%)	60.4	10.4	15.3	4.8	9.1
Region II					
Major cycles (a)	2.21	5.25	21	21	
Variance contribution rates (%)	59.2	12.1	7.2	0.6	20.9
Region III					
Major cycles (a)	2.21	3.8	21	21	
Variance contribution rates (%)	58.3	11.1	13.0	5.0	12.6

in the study region was closely related to the interdecadal oscillation of the Pacific Ocean and the East Asian summer monsoon (Wei et al. 2010).

3.2 Variation of rainfall extremes series

The 43-year extreme rainfall series (annual maximum 1-day, annual maximum 3-day, annual maximum 7-day, and annual maximum 15-day) at 61 rainfall stations in the NAHPP were calculated. The statistical characteristics of the maximum 1-day rainfall and the maximum 7-day rainfall in different stations and the statistical characteristics of the maximum 1-day rainfall and the maximum 7-day rainfall in different years are shown in Fig. 4. The number of rainfall stations is displayed in Table 2. The maximum daily rainfall of 50–100 mm in 32 stations is at rainstorm level, and the maximum daily rainfall of more than 100 mm in 29 stations is at rainstorm level. The average value of maximum

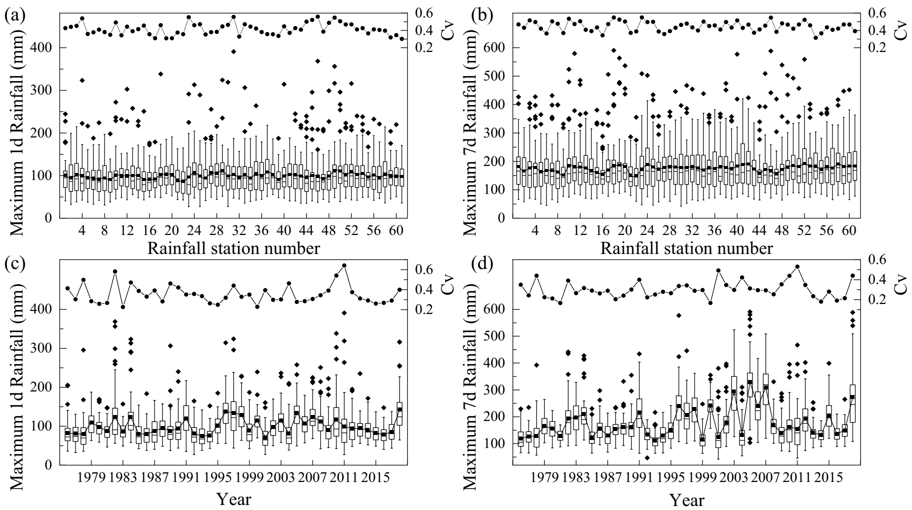

Fig. 4 Boxplot of rainfall extreme values at different stations **a**, **b** and in different years **c**, **d**

Table 2 K-S test results of maximum 1-day rainfall at different rainfall stations

Stations (Number)	Gumbel	P-III	GEV	Optimal distribution	Stations (Number)	Gumbel	P-III	GEV	Optimal distribution
Yangqiao(1)	0.106	0.091	0.085	GEV	Guzhenzha(32)	0.093	0.084	0.084	P-III, GEV
Fuyang(2)	0.086	0.093	0.093	Gumbel	Jiuwan(33)	0.127	0.136	0.093	GEV
Yingshang(3)	0.092	0.102	0.103	Gumbel	Fangdianzi(34)	0.109	0.097	0.112	P-III
Funan(4)	0.124	0.112	0.106	GEV	Baoji(35)	0.098	0.101	0.107	Gumbel
Lutaizi(5)	0.099	0.102	0.096	GEV	Xinmaqiao(36)	0.135	0.126	0.126	P-III
Zhangouji(6)	0.074	0.067	0.074	P-III	Renlou(37)	0.108	0.108	0.115	Gumbel, P-III
Fengtai(7)	0.098	0.078	0.102	P-III	Haocheng(38)	0.110	0.100	0.102	P-III
Huainan (8)	0.101	0.088	0.092	P-III	Dadian(39)	0.087	0.079	0.086	P-III
Niqiu(9)	0.122	0.105	0.108	P-III	Haogouji(40)	0.106	0.204	0.075	GEV
Guanji(10)	0.124	0.079	0.095	P-III	Shantangji(41)	0.101	0.099	0.099	P-III , GEV
Gaogongmiao(11)	0.075	0.097	0.085	Gumbel	Youji(42)	0.086	0.075	0.089	P-III
Wangshiji(12)	0.155	0.172	0.111	GEV	Xulouzha(43)	0.080	0.070	0.083	P-III
Shunheji(13)	0.106	0.073	0.105	P-III	Dangshan(44)	0.127	0.115	0.111	GEV
Boxian(14)	0.123	0.096	0.111	P-III	Gukouzha(45)	0.158	0.135	0.131	GEV
Shuanggou(15)	0.113	0.071	0.093	P-III	Zhangzhuangzhai(46)	0.173	0.200	0.118	GEV
Yimenji(16)	0.108	0.105	0.114	P-III	Huangkou(47)	0.121	0.100	0.102	P-III
Guoyang(17)	0.070	0.084	0.084	Gumbel	Jiawozha(48)	0.125	0.136	0.090	GEV
Maji(18)	0.113	0.214	0.086	GEV	Xiaoxian(49)	0.180	0.111	0.138	P-III
Mengcheng(19)	0.112	0.120	0.123	Gumbel	Yonggu(50)	0.172	0.124	0.147	P-III
Banqiaoji(20)	0.101	0.075	0.080	P-III	Fulijizha(51)	0.165	0.150	0.161	P-III
Zhangji(21)	0.102	0.088	0.089	P-III	Lingbi(52)	0.085	0.118	0.059	GEV
Lixingji(22)	0.125	0.099	0.101	P-III	Sixian(53)	0.100	0.087	0.096	P-III
Jiangzhai(23)	0.101	0.065	0.094	P-III	Huangcangyu(54)	0.121	0.094	0.109	P-III
Songji(24)	0.091	0.172	0.102	Gumbel	Chulan(55)	0.101	0.086	0.088	P-III
Zhongcungang(25)	0.115	0.084	0.107	P-III	Shicun(56)	0.095	0.082	0.100	P-III
Huaiyuan(26)	0.080	0.062	0.064	P-III	Huitanggouzha(57)	0.128	0.118	0.129	P-III
Bengbu(27)	0.089	0.091	0.083	GEV	Dazhuang(58)	0.103	0.112	0.115	Gumbel

Table 2 (continued)

Stations (Number)	Gumbel	P-III	GEV	Optimal distribution	Stations (Number)	Gumbel	P-III	GEV	Optimal distribution
Mohekou(28)	0.072	0.060	0.066	P-III	Baishaji(59)	0.086	0.084	0.084	P-III , GEV
Fushan(29)	0.100	0.135	0.066	GEV	Nanpingzha(60)	0.085	0.081	0.082	P-III
Longkangji(30)	0.108	0.198	0.078	GEV	Huazhuangji (61)	0.090	0.060	0.058	GEV
Heliu(31)	0.119	0.198	0.068	GEV					

1-day rainfall and the average value of maximum 7-day rainfall fluctuated little at the different stations (Fig. 4a, b), and the difference between the average value and the maximum value is large. In general, the variation coefficient (CV) of the two extreme value series is between 0.3 and 0.5, but the CV value of the maximum 7-day rainfall at the same station is slightly higher than that of the maximum 1-day rainfall. It can also be found from the anomaly points that the maximum 7-day rainfall has many abnormal points. The degree of dispersion is large. The results show that the distribution of the extreme value of rainfall is not uniform at a different time at the same station. In different years, the extreme value of rainfall varies greatly (Fig. 4c, d), as does the mean value. Moreover, the maximum 1-day rainfall and the maximum 7-day rainfall CV easily appear at the extreme point. The spatial distribution is quite different at this extreme point.

In spatial distribution, the maximum 1-day rainfall $C_V=0.06$ and the maximum 7-day rainfall $C_V=0.06$ in the NAHPP. In temporal distribution, the maximum 1-day rainfall $C_V=0.2$ and the maximum 7-day rainfall $C_V=0.3$ in the NAHPP. According to the classification standard of C_V (Wu et al. 2011), the rainfall extremes show weak variation ($C_V<0.1$) in spatial distribution, and the rainfall extreme value shows a medium variation ($0.1<C_V<1$) in time distribution, which indicates that the temporal variation of rainfall extreme value in the NAHPP is higher than the spatial variation. The results are consistent with the variation range of the mean in Fig. 2. In all kinds of extreme hydrometeorology, spatial and temporal changes are very complex (Jung et al. 2017). The NAHPP is located in a transitional zone between the north and the south, and the influence of climate on rainfall is more complex.

In order to study the influence of geographical location on extreme rainfall (Fig. 5), the relationship between the extreme rainfall and latitude/longitude was analyzed by regression analysis. As displayed in Fig. 5a, b, the maximum 1-day rainfall correlated positively with longitude ($R2 = 0.17$), while the maximum 1-day rainfall was not correlated with latitude.

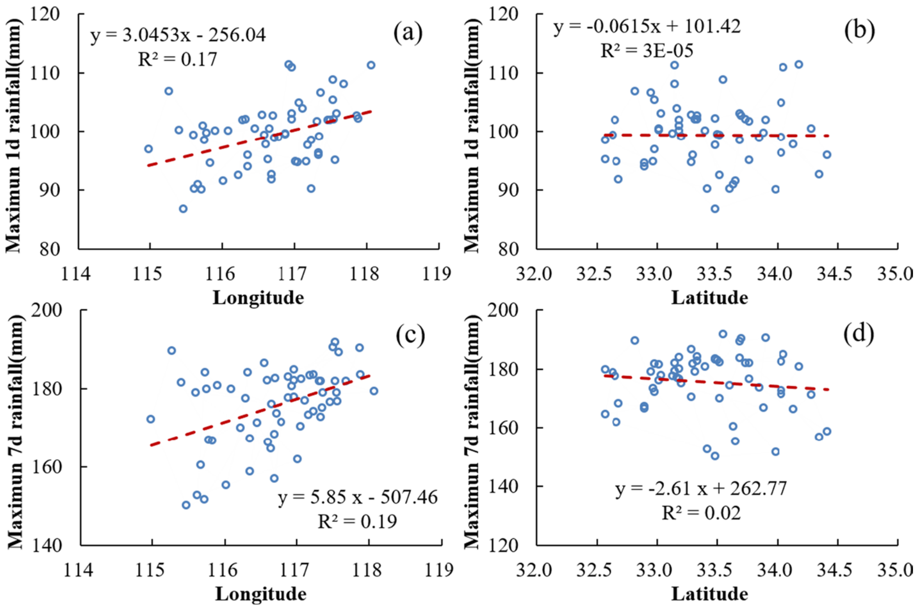

Fig. 5 Linear relationship between rainfall extreme value and longitude/latitude

As a result, in Fig. 5c, d, there was a significant positive correlation between the maximum 7-day rainfall and longitude ($R2 = 0.19$), and a very weak negative correlation between the maximum 7-day rainfall and latitude ($R2 = 0.02$). Thus, the extreme value of rainfall in the NAHPP increases with longitude and had little correlation with latitude. This conclusion is consistent with the shape characteristics of the boundary of the NAHPP (east–west long, north–south short). Longitude has great influence on the extreme value of rainfall. It is further proved that the spatial distribution of rainfall extremes in this area is not uniform.

The MK trend test method was used to analyze the variation trend of rainfall extreme values in the NAHPP during 1976 and 2018, and the analysis results are shown in Fig. 6. The date of annual maximum daily rainfall of each station in the past 43 years was also calculated. For the whole NAHPP, the MK test indicated an insignificant increasing trend in different rainfall extremes series. Taking the annual maximum daily rainfall and annual maximum 3-day rainfall as examples, the changing trend of a single station was analyzed.

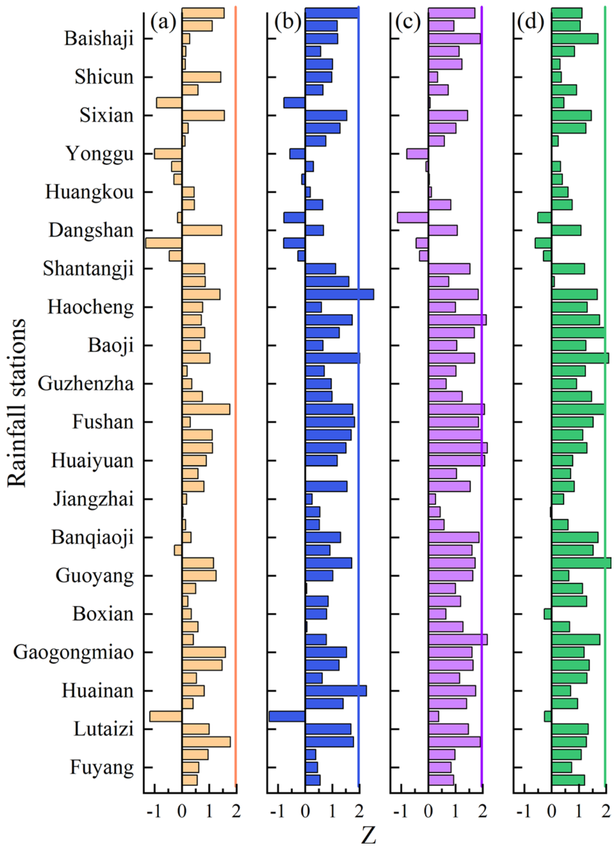

Fig. 6 MK test results for each rainfall station. **a** Maximum 1-day rainfall; **b** Maximum 3-day rainfall; **c** Maximum 7-day rainfall; **d** Maximum 15-day rainfall;

Among the 61 rainfall stations, the annual maximum daily rainfall showed increasing trend in 52 stations and decreasing trend in 9 stations, all of which showed no significant (α= 0.05) change (Fig. 6). Furthermore, the maximum daily rainfall mainly occurred between 1990 and 2010. The maximum 3-day rainfall showed an increasing trend in 54 stations, among which three stations showed a significant increasing trend (Fangdianzi, Dadian, and Huazhuangji), and seven stations showed no significant decreasing trend. Interestingly, Youji, Xuxialou, Gukouzha, and Yonggu showed no significant decreasing trends in four different rainfall extremes series (Fig. 6).

The rainfall extremes in the NAHPP showed no significant increasing trend. Although there is an increasing trend of precipitation in the NAHPP, the change is insignificant. The maximum 1-day rainfall at most stations showed nonsignificant increase trend, and a few stations showed nonsignificant decrease trend (Fig. 6). This is consistent with the results of Xia et al. (2012). The average annual precipitation increase in the HRB is 1.2 mm/10a, but the number of precipitation days decreases, and the radiation decrease is 0.8/10d (Wang et al. 2016). It should be noted that individual rainfall is increasing, which increases the risk of flooding. In addition, Zhang et al. (2014) have studied the HRB and suggested that the areas with the highest daily rainfall were along the middle and upper reaches of the HRB. The number of extreme precipitation days and precipitation intensity has an increasing trend (Ye and Li 2017). Moreover, the high-risk areas for rainstorms and floods in the HRB include Funan County in the NAHPP. The strong precipitation anomaly in the HRB may be related to the East Asian summer monsoon and the unique circulation pattern in East Asia (Wei and Zhang 2010). More importantly, there is a positive correlation between flooding and temperature in the HRB, with a positive coefficient of 0.88, and temperatures are expected to increase even faster in the future (Yang et al. 2012). Consequently, the flood disaster risk in the NAHPP cannot be ignored.

3.3 Probability distribution functions of rainfall extremes

The Gumbel, P-III, and GEV distribution functions were used to fit the four types of rainfall extremes series (maximum 1-day, maximum 3-day, maximum 7-day, and maximum

Table 3 Proportion (station numbers) of optimal fitting distribution function of extreme rainfall

Distribution function	Extreme rainfall			
	Maximum 1d rainfall	Maximum 3d rainfall	Maximum 7d rainfall	Maximum 15d rainfall
Gumbel	15% (9)	25% (15)	25% (15)	20% (12)
P-III	59% (36)	52% (32)	54% (33)	66% (40)
GEV	33% (20)	25% (15)	25% (15)	18% (11)

15-day rainfall), and the K-S test evaluated the goodness of fit of the three distribution functions. The K-S statistical value of maximum 1-day rainfall is presented in Table 2. The D value fitted by P-III distribution at Maji station ($D=0.214$) did not pass the significance level test ($\alpha = 0.05$), but all the other stations did ($\alpha = 0.05$). The best fitted distribution functions of extreme rainfall are presented in Table 3. It can be found that the P-III distribution function accounts for the largest proportion of the optimal fitting distribution function of extreme rainfall, accounting for 52–66% (the number of rainfall stations is between 32 and 40). So, in this study, P-III distribution function can well fit the maximum 1-day, 3-day, 7-day, and 15-day precipitation in the NAHPP (Tables 2, 3). Hanson and Vogel (2008) obtained the same results for maximum 1-day precipitation data analysis. Especially in the maximum 15-day rainfall, the effect of P-III distribution fitting is more prominent.

In terms of annual maximum daily rainfall, 36 stations conformed to the P-III distribution, accounting for 59% of the total number of stations, 20 stations conformed to the GEV distribution, accounting for 33% of the total number of stations, and nine stations conformed to the Gumbel distribution, accounting for 15% of the total number of stations. (The optimal distribution is repeatedly counted.) Compared with the P-III and GEV distribution functions, the Gumbel distribution is not suitable for simulating the maximum 1-day rainfall in the NAHPP. Yang et al. (2010) and Khudri and Sadia (2013) have revealed the appearance of several opposite themes. Yang et al. (2010) analyzed the annual rainfall of 1-, 3-, 5-, and 7-day in the Pearl River Basin and found that GEV distribution function is one of the best fitting distribution functions. Khudri and Sadia (2013) found that the GEV and four parameters generalized Gamma distribution can well fit the annual maximum rainfall data of 22 weather stations in Bangladesh. The reason for this difference may be closely related to the local climate characteristics (Valenzuela and Garreaud 2019). Therefore, estimating the distribution of extreme rainfall in different regions is of great significance to accurately assess extreme rainfall.

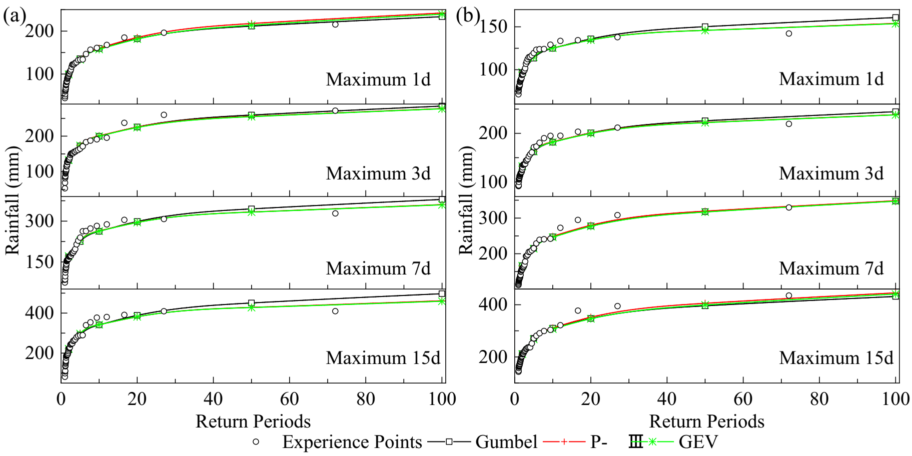

Fig. 7 Comparison of the theoretical and empirical return periods of Bengbu **a** and NAHPP **b**

3.4 Return period of rainfall extremes

Through three distribution functions, the rainfall of each station in different return periods (5a, 10a, 20a, 50a, and 100a) was calculated, and the optimal distribution function of the rainfall extremes value was obtained. The results were compared with the empirical return periods of samples (Fig. 7). It is clear that the fitting results of theoretical return periods and empirical return periods obtained by the three distribution functions are good for both individual stations and the NAHPP. Among them, the fitting results of the P-III and GEV distributions are very close to the extreme values of rainfall and are close to the empirical return period fitting results (Fig. 7). However, the Gumbel distribution correlated poorly, which is consistent with the K-S test results. The fitting results of three distribution functions of maximum 7-day rainfall are the closest. But when the return period is 10a, the fitting results of the three distribution functions and the empirical return period are unideal. When the return periods are 50a and 100a, the calculated extreme values of rainfall are slightly larger than those in the empirical return periods, which help to avoid the risk of flooding.

According to the results of the K-S test and the fitting of the theoretical and empirical return periods, the rainfall in different return periods was estimated by using the better fitting P-III distribution. Then, the inverse distance weighting method in ArcGIS was used for spatial interpolation, and the spatial distribution of rainfall extremes in different return periods in the NAHPP was obtained (Fig. 8). As a result, in Fig. 8, the return periods of different extreme values are consistent. When the return period is 50a, the maximum value of the maximum 1-day rainfall mainly occurs in the northern NAHPP. Only some stations have relatively large rainfall (Xiaoxian and Heliu stations), and the difference between stations can reach 140 mm (Fig. 8a). It can be seen that the spatial distribution of rainfall in the NAHPP is uneven. The maximum value of the maximum 1-day rainfall mainly occurs in the southwestern NAHPP (Fig. 8c). The maximum values of the maximum 7-day rainfall (Fig. 8e) and the maximum 15-day rainfall mainly occur in the central NAHPP (Fig. 8g). The migration path of extreme rainfall is: north-southwest-central-central. The trend of rainfall extremes with a 100a return period is similar to that with a 50a return period.

The temporal and spatial variability of extreme rainfall is very complex. Although much work has been done on the coupling of rainfall dynamics and statistical description, the results obtained are not accurate (Bougadis and Adamowski 2006). Therefore, a scaling model was proposed to test the scale variability of extreme rainfall time series (Bougadis and Adamowski 2006). Nevertheless, there is no consensus on which distribution function to use in extreme rainfall. At present, the most widely used distribution functions are the GEV, Gumbel, P-III, Gamma, and Weibull distributions. Papalexiou et al. (2013) reported the applicability of several probability distribution models in global extreme daily rainfall and pointed out that the GEV distribution can be used to estimate the frequency of extreme daily rainfall. One of the focuses of this paper is to determine the probability distribution function suitable for the NAHPP, and our results indicate that the P-III distribution function has the best adaptability, followed by the GEV distribution function (Table 2 and Fig. 7). Using the P-III distribution function, the rainfall extreme value distribution under different return periods was calculated. The maximum 1-day rainfall in the 2-year return period is mostly less than 100 mm, and only two stations have rainfall of more than 100 mm. The maximum 1-day rainfall in the 5-year return period, 10-year return period, 20-year return period, and 50-year return period is basically 100–250 mm, and there are more stations

Fig. 8 Distribution of rainfall extremes in different return periods in the NAHPP.**a** maximum 1-day rainfall, return period 50a; **b** maximum 1-day rainfall, return period 100a; **c** maximum 3-day rainfall, return period 50a; **d** maximum 3-day rainfall, return period 100a; **e** maximum 7-day rainfall, return period 50a; **f** maximum 7-day rainfall, return period 100a; **g** maximum 15-day rainfall, return period 50a; **h** maximum 15-day rainfall, return period 100a

with rainfall of over 250 mm in the maximum 1-day rainfall of 100-year return period, reaching the level of torrential rain.

Rainfall extremes are highly related to crop yields. Previous studies indicate that if groundwater level drops to 0.5 m below ground surface in three days after a rain storm, the rainstorm event will have little effect on crop yield. Otherwise, crop production will probably decrease to a certain extent (Wang and Ye 2008). If the drainage time exceeds three days, the crop yield will fall. Therefore, studying the distribution of rainfall extreme values can help improve farmland drainage in this area.

4 Conclusions

Based on observed rainfall data at 61 rainfall stations in the NAHPP from 1978 to 2018, temporal change trends and spatial distributions of the annual maximum 1-day, 3-day, 7-day, and 15-day rainfall in the NAHPP were analyzed by using the KCA, EEMD, MK, and K-S methods. Furthermore, the probability distribution of rainfall extremes in the NAHPP was investigated by using the Gumbel, P-III, and GEV models. This study can be concluded as follows:

(1) The contribution of the oscillation period of 2.2–2.3 years to the rainfall anomaly was the largest (more than 58%), and rainfall shows a 2–3-year periodicity on the interannual scale and 21-year periodicity on the chronological scale.

(2) The rainfall extremes in the NAHPP showed a weak variation in spatial distribution, and the rainfall extreme value showed a medium variation in time distribution. The spatial distribution of rainfall extremes in this area was not uniform, and the rainfall extremes in the NAHPP increased with longitude and had little correlation with latitude. The rainfall extremes showed nonsignificant increase trend over the whole NAHPP, but some stations showed nonsignificant decrease trend.

(3) The D value fitted by P-III distribution at Maji station ($D = 0.214$) did not pass the significance level test ($\alpha = 0.05$), but all other stations did ($\alpha = 0.05$). The P-III distribution function can fit the extreme value of rainfall (the maximum 1-day rainfall: 59%), followed by the GEV distribution function (the maximum 1-day rainfall: 33%). It is recommended to use the P-III distribution function to fit rainfall extremes in the study area.

(4) As the return period increased, the rainfall estimates using the three distribution functions were slightly larger than that in the empirical return period. The findings can provide scientific support on flood control standard design and flood risk mitigation.

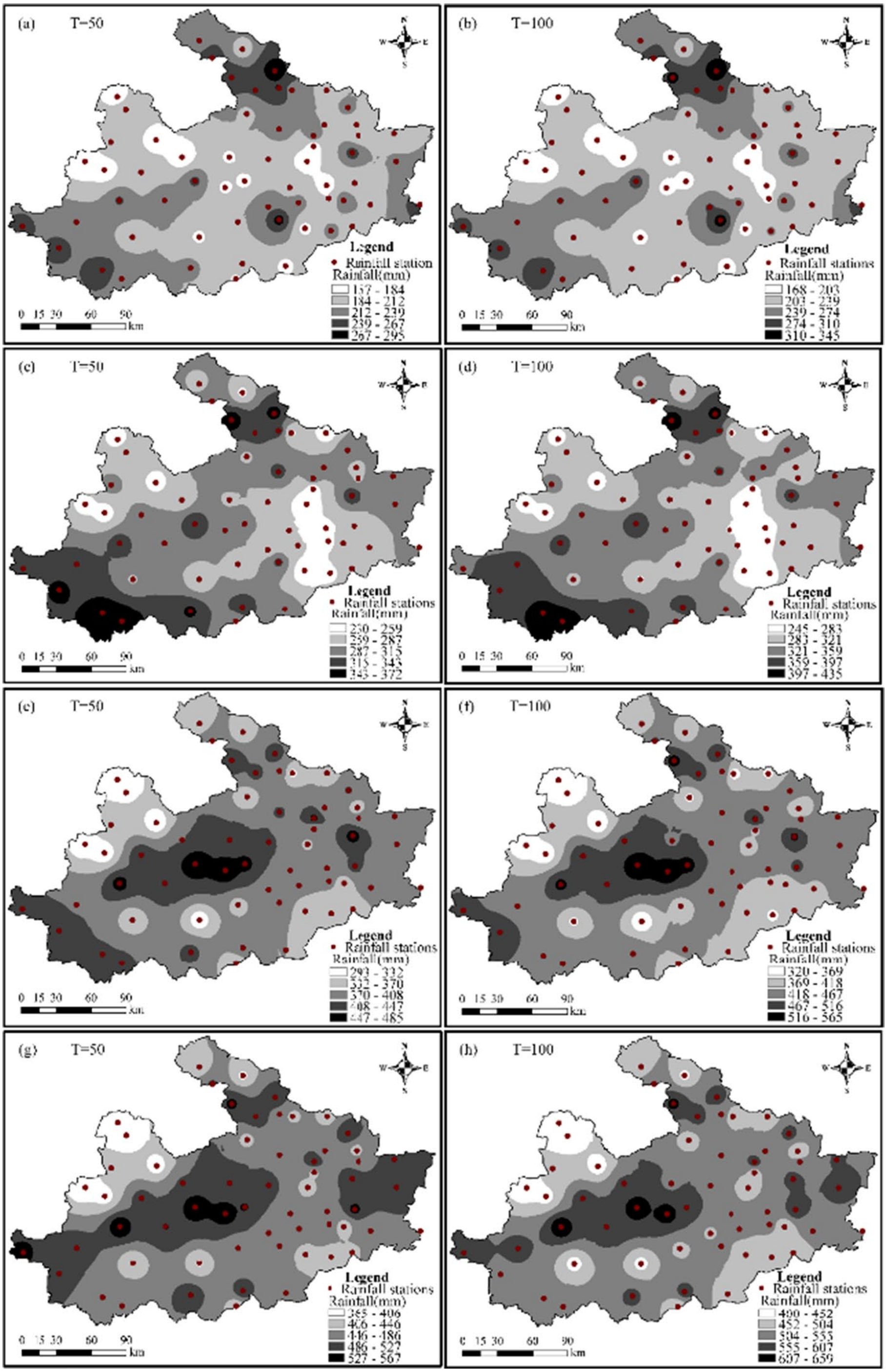
(a) T=50
Legend
Rainfall station
Rainfall(mm)
157 - 184
184 - 212
212 - 239
239 - 267
267 - 295
(b) T=100
Legend
Rainfall stations
Rainfall(mm)
168 - 203
203 - 239
239 - 274
274 - 310
310 - 345
(c) T=50
Legend
Rainfall stations
Rainfall(mm)
230 - 259
259 - 287
287 - 315
315 - 343
343 - 372
(d) T=100
Legend
Rainfall stations
Rainfall(mm)
245 - 283
283 - 321
321 - 359
359 - 397
397 - 435
(e) T=50
Legend
Rainfall stations
Rainfall(mm)
293 - 332
332 - 370
370 - 408
408 - 447
447 - 485
(f) T=100
Legend
Rainfall stations
Rainfall(mm)
320 - 369
369 - 418
418 - 467
467 - 516
516 - 565
(g) T=50
Legend
Rainfall stations
Rainfall(mm)
365 - 406
406 - 446
446 - 486
486 - 527
527 - 567
(h) T=100
Legend
Rainfall stations
Rainfall(mm)
400 - 452
452 - 504
504 - 555
555 - 607
607 - 659
0 15 30 60 90 km
N
W E
S

Acknowledgements This study has been financially supported by the National Key Research and Development Programs of China (Grant number: 2016YFA0601501), the National Natural Science Foundation of China (Grant numbers: 41830863, 51879162, 51879164, 51779144, 52079026, and 91747103), and the Belt and Road Fund on Water and Sustainability of the State Key Laboratory of Hydrology-Water Resources and Hydraulic Engineering (Grant Number: 2019nkzd02). We also appreciate two anonymous reviewers for their valuable comments and Ms. Samantha Kierath for her kind assistance to proofread the revised manuscript.

Author contributions JZ and GW designed the study and improved the manuscript; MD performed the data analysis and drafted the paper; ZW and ZB reviewed the designed study and methods; CL and JJ collected data and conducted results analysis; YL and QY revised the manuscript and provided discussion on results.

Compliance with ethical standards

Conflict of interests The authors declare that they have no conflict of interests.

References

Amiri MA, Mesgari MS (2016) Spatial variability analysis of precipitation in northwest Iran. Arab J Geosci. https://doi.org/10.1007/s12517-016-2611-7

Bougadis J, Adamowski K (2006) Scaling model of a rainfall intensity-duration-frequency relationship. Hydrol Process 20(17):3747–3757

Boukhelifa M, Meddi M, Gaume E (2018) Integrated bayesian estimation of intensity-duration frequency curves: consolidation and extensive testing of a method. Water Resour Res 54(10):7459–7477

Chen BL, Zhu YH, Wang CY, Lu HS (2018) Spatiotemporal variation of precipitation and evapotranspiration in Huaibei plain. J Irrig Drain 37(6):109–116 (in Chinese with English abstract)

Chaudhuri RR, Sharma P (2020) Addressing uncertainty in extreme rainfall intensity for semi-arid urban regions: case study of Delhi. Nat Hazards, India. https://doi.org/10.1007/s11069-020-04273-5

Coronado-Hernández ÓE, Merlano-Sabalza E, Díaz-Vergara Z, Coronado-Hernández JR (2020) Selection of hydrological probability distributions for extreme rainfall events in the regions of Colombia. Water. https://doi.org/10.3390/w12051397

Cunnane C (1978) Unbiased plotting positions-a review. J Hydrol 37(3–4):205–222

Diffenbaugh NS, Singh D, Mankin JS, Horton DE, Swain DL, Touma D, Charland A, Liu YJ, Haugen M, Tsiang M (2017) Quantifying the influence of global warming on unprecedented extreme climate events. Proc Natl Acad Sci USA 114:4881–4886

Dinpashoh Y, Jahanbakhsh-Asl S, Rasouli AA, Foroughi M, Singh VP (2019) Impact of climate change on potential evapotranspiration (case study: west and NW of Iran). Theor Appl Climatol 136(1–2):185–201

Du H, Xia J, Zeng SD, She DX, Liu JJ (2014) Variations and statistical probability characteristic analysis of extreme precipitation events under climate change in Haihe River Basin China. Hydrol Process 28(3):913–925

Duan WL, He B, Takara K, Luo PP, Nover D, Yamashiki Y, Huang WR (2014) Anomalous atmospheric events leading to Kyushu's flash floods, July 11–14. Nat Hazards 73(3):1255–1267

Fan J, Sun WC, Zhao Y, Xue BL, Zuo DP, Xu ZX (2018) Trend analyses of extreme precipitation events in the Yarlung Zangbo River Basin. Sustainability, China Using a High-Resolution Precipitation Product. https://doi.org/10.3390/su10051396

Fischer T, Su B, Luo Y, Scholten T (2012) Probability distribution of precipitation extremes for weather index–based insurance in the Zhujiang River Basin South China. J Hydrometeorol 13(3):1023–1037

Guhathakurta P, Sreejith OP, Menon PA (2011) Impact of climate change on extreme rainfall events and flood risk in India. J Earth Syst Sci 120(3):359–373

Ge J, You QL, Zhang YQ (2019) Effect of Tibetan Plateau heating on summer extreme precipitation in eastern China. Atmos Res 218:364–371

Hanson LS, Vogel R (2008) The Probability Distribution of Daily Rainfall in the United States. World Environmental and Water Resources Congress, Honolulu

Hosseinzadehtalaei P, Tabari H, Willems P (2019) Regionalization of anthropogenically forced changes in 3 hourly extreme precipitation over Europe. Environ Res Lett. https://doi.org/10.1088/1748-9326/ab5638

Hosseinzadehtalaei P, Tabari H, Willems P (2020) Climate change impact on short-duration extreme precipitation and intensity–duration–frequency curves over Europe. J Hydrol. https://doi.org/10.1016/j.jhydrol.2020.125249

Huang NE, Wu ZH, Pinzón JE, Parkinson CL, Long SR, Blank K, Gloersen P, Chen XY (2009) Reductions of noise and uncertainty in annual global surface temperature anomaly data. Adv Adapt Data Anal 1(3):447–460

IPCC, Climate Change (2013) The Physical Science Basis[M]. Cambridge University Press, Cambridge, p 2013

Jin SY, Gao YJ, Xu JH (2019) Impact of series length and maximum processing on estimation of rainfall return period. J China Hydrol 39(5):25–29 (**in Chinese with English abstract**)

Jin XX, Sun Y, Li C, Yang TY (2014) Precipitation and the features of atmospheric circulation in the Huaihe River Basin in recent 50 years. Resour Environ Yangtze Basin 23(5):609–616 (in Chinese with English abstract)

Jung I, Bae D, Kim G (2011) Recent trends of mean and extreme precipitation in Korea. Int J Climatol 31(3):359–370

Jung YH, Shin JY, Ahn HJ, Heo JH (2017) The Spatial and temporal structure of extreme rainfall trends in South Korea. Water. https://doi.org/10.3390/w9100809

Khudri MM, Sadia F (2013) Determination of the best fit probability distribution for annual extreme precipitation in Bangladesh. Eur J Sci Res 103:391–404

McAfee SA, Guentchev G, Eischeid JK (2013) Reconciling precipitation trends in Alaska: 1. Station-based analyses. J Geophys Res Atmos 118(14):7523–7541

Merabti A, Martins DS, Meddi M, Pereira LS (2018) Spatial and time variability of drought based on SPI and RDI with various time scales. Water Resour Manag 32(3):1087–1100

Min S, Zhang X, Zwiers FW, Hegerl GC (2011) Human contribution to more-intense precipitation extremes. Nature 470:378–381

Mo CX, Ruan YL, He JQ, Jin JL, Liu P, Sun GK (2019) Frequency analysis of precipitation extremes under climate change. Int J Climatol 39(3):1373–1387

Ntegeka V, Willems P (2008) Trends and multidecadal oscillations in rainfall extremes, based on a more than 100-year time series of 10 min rainfall intensities at Uccle Belg. Water Resour Res 44(7):19–33

Olsson J, Berg P, Kawamura A (2015) Impact of RCM spatial resolution on the reproduction of local, subdaily precipitation. J Hydrometeorol 16(2):534–547

Panthou G, Vischel T, Lebel T (2014) Recent trends in the regime of extreme rainfall in the Central Sahel. Int J Climatol 34(15):3998–4006

Papalexiou SM, Koutsoyiannis D (2013) Battle of extreme value distributions: a global survey on extreme daily rainfall. Water Resour Res 49(1):187–201

Park J, Kang H, Lee YS, Kim M (2011) Changes in the extreme daily rainfall in South Korea. Int J Climatol 31(15):2290–2299

Qian LX, Wang HR, Dang SZ, Wang C, Jiao ZQ, Zhao Y (2018) Modelling bivariate extreme precipitation distribution for data-scarce regions using Gumbel-Hougaard copula with maximum entropy estimation. Hydrol Process 32(2):212–227

Rahman AS, Rahman A, Zaman MA, Haddad K, Ahsan A, Imteaz M (2013) A study on selection of probability distributions for at-site flood frequency analysis in Australia. Nat Hazards 69(3):1803–1813

Sarhadi A, Soulis ED (2017) Time-varying extreme rainfall intensity-duration-frequency curves in a changing climate. Geophys Res Lett 44(5):2454–2463

Samuel BS, Agog NS, Peter M, Abdullateef M, Kwaghdoo AG (2020) Modeling extreme rainfall in Kaduna using the generalised extreme value distribution. Sci World J 15(3):73–77

Shu ZK, Liu J, Dong XH, Yu D (2017) Distribution of staged extreme rainfalls in flood season based on fuzzy set analysis. J Hydroelectr Eng 36(7):55–64 (**in Chinese with English abstract**)

Soltani M, Laux P, Kunstmann H, Stan K, Sohrabi MM, Molanejad M, Sabziparvar AA, Ranjbar Saadatabadi A, Ranjbar F, Rousta I (2016) Assessment of climate variations in temperature and precipitation extreme events over Iran. Theor Appl Climatol 126(3):775–795

Song XM, Zhang JY, Kong FZ (2018) Probability distribution of extreme precipitation in Beijing based on extreme value theory. Scientia Sinica Technologica 48(6):639–650 (**in Chinese with English abstract**)

Tong RZ, Sun WC, Han Q, Yu JS, Tian ZF (2020) Spatial and temporal variations in extreme precipitation and temperature events in the Beijing–Tianjin–Hebei region of China over the past six decades. Sustainability. https://doi.org/10.3390/su12041415

Valenzuela RULA, Garreaud RED (2019) Extreme daily rainfall in central-southern Chile and its relationship with low-level horizontal water vapor fluxes. J Hydrometeorol 20(9):1829–1850
Wang F, Tian H (2010) Characteristics of extreme precipitation events in Huaihe River Basin in 1960–2007. Clim Change Res 6(3):228–229 (in Chinese with English abstract)
Wang Y, Cheng C, Xie Y, Liu B, Yin S, Liu Y, Hao Y (2017) Increasing trends in rainfall-runoff erosivity in the source region of the Three Rivers, 1961–2012. Sci Total Environ 592:639–648
Wang Y, Zhang Q, Zhang S, Chen XH (2016) Spatial and temporal characteristics of precipitation in the Huaihe River Basin and its response to ENSO events. Scientia Geographica Sinica 36(1):128–134 (in Chinese with English abstract)
Wang W, Chen X, Shi P, Van Gelder PHAJ, Corzo G (2008) Extreme precipitation and extreme streamflow in the Dongjiang River Basin in southern China. Hydrol Earth Syst Sci 12:207–221
Wang YZ, Ye NJ (2008) Drainage of farmland in Huaibei Plain of Anhui Province. China Rural Water Hydropower 2:5–7 (in Chinese with English abstract)
Wei FY, Zhang T (2010) Oscillation characteristics of summer precipitation in the Huaihe River valley and relevant climate background. Sci China Earth Sci 53(2):301–316
Westra S, Alexander LV, Zwiers FW (2013) Global increasing trends in annual maximum daily precipitation. J Clim 26(11):3904–3918
Wu CG, Lin DS, Xiao WF, Wang PC, Ma H, Zhou ZX (2011) Spatiotemporal distribution characteristics of rainfall erosivity in three Gorges Reservoir Area. Chin J Appl Ecol 22(1):151–158 (in Chinese with English abstract)
Wu HC, Yang QL, Liu JM, Wang GQ (2020) A spatiotemporal deep fusion model for merging satellite and gauge precipitation in China. J Hydrol. https://doi.org/10.1016/j.jhydrol.2020.124664
Wu ZH, Huang NE (2009) Ensemble empirical mode decomposition: A noise-assisted data analysis method. Adv Adapt Data Anal 1(1):1–41
Wu X, Guo S, Yin J, Yang G, Zhong Y, Liu D (2018) On the event-based extreme precipitation across China: time distribution patterns, trends, and return levels. J Hydrol 562:305–317
Xia J, She D, Zhang Y, Du H (2012) Spatio-temporal trend and statistical distribution of extreme precipitation events in Huaihe River Basin during 1960–2009. J Geogr Sci 22(2):195–208
Yang CG, Yu ZB, Hao ZC, Zhang JY, Zhu JT (2012) Impact of climate change on flood and drought events in Huaihe River Basin. China Hydrol Res 43(1–2):14–22
Ye ZW, Li ZH (2017) Spatiotemporal variability and trends of extreme precipitation in the Huaihe River Basin, a climatic transitional zone in East China. Adv Meteorol. https://doi.org/10.1155/2017/3197435
Yang M, Chen X, Cheng CS (2016) Hydrological impacts of precipitation extremes in the Huaihe River Basin. SpringerPlus, China. https://doi.org/10.1186/s40064-016-3429-1
Yin J, Yan DH, Yang ZY, Yuan Z, Yuan Y, Zhang C (2016) Projection of extreme precipitation in the context of climate change in Huang-Huai-Hai region. China J Earth Syst Sci 125(2):417–429
Yang T, Shao QX, Hao ZC, Chen X, Zhang ZX, Xu CY, Sun LM (2010) Regional frequency analysis and spatio-temporal pattern characterization of rainfall extremes in the Pearl River Basin. China J Hydrol 380(3–4):386–405
Zhang ZT, Gao C, Liu Q, Zhai JQ, Wang YJ, Su BD, Tian H (2014) Risk assessment on storm flood disasters of different return periods in Huaihe River basin. Geogr Res-Aust 33(7):1361–1372 (in Chinese with English abstract)

Publisher's Note Springer Nature remains neutral with regard to jurisdictional claims in published maps and institutional affiliations.

Affiliations

Mingcheng Du[1,2] · Jianyun Zhang[1,2,3,4] · Qinli Yang[5] · Zhenlong Wang[6,7] · Zhenxin Bao[2,3,4] · Yanli Liu[2,3,4] · Junliang Jin[2,3,4] · Cuishan Liu[2,3,4] · Guoqing Wang[2,3,4]

Mingcheng Du
mingchengd@163.com

Jianyun Zhang
jyzhang@nhri.cn

Qinli Yang
qinli.yang@uestc.edu.cn

Zhenlong Wang
gqwang@nhri.cn

Zhenxin Bao
zxbao@nhri.cn

Yanli Liu
ylliu@nhri.cn

Junliang Jin
jljin@nhri.cn

Cuishan Liu
csliu@nhri.cn

[1] School of Civil Engineering, Tianjin University, Tianjin 300350, China

[2] State Key Laboratory of Hydrology-Water Resources and Hydraulic Engineering, Nanjing Hydraulic Research Institute, Nanjing 210029, China

[3] Yangtze Institute for Conservation and Development, Nanjing 210098, China

[4] Research Center for Climate Change, Nanjing 210029, China

[5] University of Electronic Science and Technology of China, Chengdu 611731, China

[6] Wudaogou Experimental Station for Hydrology and Water Resources, Bengbu 233704, China

[7] Huai River Commission, Anhui Hydraulic Research Institute, Bengbu 233000, China